



ELSEVIER

Available online at www.sciencedirect.com

SCIENCE @ DIRECT®

Nuclear Instruments and Methods in Physics Research A 543 (2005) 483–496

NUCLEAR
INSTRUMENTS
& METHODS
IN PHYSICS
RESEARCH
Section A

www.elsevier.com/locate/nima

Correlated measurements of secondary cosmic ray fluxes by the Aragats Space-Environmental Center monitors

A. Chilingarian*, K. Arakelyan, K. Avakyan, V. Babayan, N. Bostanjyan, S. Chilingarian, V. Danielyan, A. Daryan, A. Egikyan, V. Eganov, G. Gharagozyan, S. Ghazaryan, T. Hairapetyan, A. Hovhanissyan, T. Hovhannissyan, V. Ivanov, G. Karapetyan, G. Kostanyan, L. Kozliner, N. Gevorgyan, H. Martirosian, L. Melkumyan, M. Nazaryan, A. Reimers, G. Rostomyan, S. Tserunyan, M. Zazyan

Cosmic Ray Division, Alikhanyan Physics Institute, Alikhanyan Brother 2, Yerevan 36, Armenia

Received 12 November 2004; accepted 12 December 2004

Available online 25 January 2005

Abstract

The Aragats Space-Environmental Center provides monitoring of different species of secondary cosmic rays at two altitudes and with different energy thresholds. One-minute data is available on-line from <http://crdlx5.yerphi.am/DVIN/index2.php>. We present description of the main monitors along with data acquisition electronics. Also we demonstrate the sensitivity of the different species of secondary cosmic ray flux to geophysical conditions, taking as examples the extremely violent events of October–November 2003. We introduce correlation analysis of the different components of registered time-series as a new tool for the classification of the geoeffective (events on

Abbreviations: ACE, Advanced Composition Explorer; AMMM, Aragats Multidirectional Muon Monitor; ArNM, Aragats Neutron Monitor; ASEC, Aragats Space Environmental Center; AU, Astronomical unit (distance Sun–Earth, 1.5×10^{11} m); CME, Coronal Mass Ejection; CR, Cosmic Rays; CRD, Cosmic Ray Division, Yerevan Physics Institute; EAS, Extensive Air Showers; ESA, European Space Agency; Fd, Forbush decrease; GAMMA, EAS installation on Mt. Aragats; GCR, Galactic Cosmic Rays; GLE, Ground level Enhancement (Excess, Event); GOES, Geostationary Operational Environmental Satellite; GPS, Global Positioning System; IMF, Interplanetary Magnetic Field; MAKET ANI, EAS installation on Mt. Aragats; NANM, Nor-Amberd Neutron Monitor; NAMMM, Nor-Amberd Multidirectional Muon Monitor; nT, nano Tesla; SNT, Solar Neutron Telescope; SEP, Solar Energetic Particles; SF, Solar Flare

*Corresponding author. Tel.: 374 1 344 377.

E-mail address: chili@crdlx5.yerphi.am (A. Chilingarian).

earth affected by solar activity) events and for the forecasting of the severity of the upcoming geomagnetic storm.

© 2005 Published by Elsevier B.V.

PACS: 95.55.Vj; 96.40.Cd; 96.40.Kk; 95.75.Pq

Keywords: Space weather; Cosmic rays; Geomagnetic storms

1. Introduction

Radiation and geomagnetic storms, which are elements of space weather, are part of the major obstacles for space operations. Reliable forecasting of the arrival of these dangerous elements is of vital importance for orbiting flights and some surface industries. In addition to the fleet of space-born instruments, worldwide networks of particle detectors spread along different latitudes and longitudes, provide valuable information on the intensity and anisotropy of the variable cosmic ray fluxes. The geomagnetic storms are driven by the shocks followed by magnetized plasma clouds, with southward magnetic field, reaching the earth. During their travel in the interplanetary space the shocks interact with the Galactic Cosmic Rays (GCR) filling the space uniformly and isotropically. As a result the angular distribution and density of GCR with energies up to hundreds of GeV will be modulated. Due to the relativistic speeds of these particles, the information on the upcoming severe disturbance of the Interplanetary Magnetic Field (IMF) is transmitted quickly and can be detected by the world-wide networks of Neutron Monitors (NM, responding to GCR energies ≥ 10 GeV) and Muon Telescopes (MT, responding to GCR energies ≥ 50 GeV) well before the onset of a major geomagnetic storm [3,11,15]. The strength of the geomagnetic storms depends on the magnitude and space distribution of the cloud's "frozen" magnetic fields. Information on the anisotropy of muons and neutrons generated in the atmosphere by the GCR provides the appropriate tool for "looking" inside the magnetized cloud far before it reaches the Earth and the L1 point, where different measuring facilities, hosted by ACE and SOHO space stations are located.

The changing intensity of the GCR also reflects the large-scale structure of the IMF and the diurnal variability of cosmic rays detected by surface monitors and has a rather complicated shape [12]. That is the reason why we need multivariate, multidetector measurements of as many components of the changing secondary cosmic rays as possible. A sudden correlated variation in the flux of neutrons, muons, and electrons, detected by the surface monitors could be an indication of an upcoming severe radiation or geomagnetic storms.

Starting from 1996 we are developing various detectors to measure fluxes of different components of secondary cosmic rays at the Aragats research stations of the Alikhanian Physics Institute (formerly known as Yerevan Physics Institute). After being down for a few years due to the economic hardships in the years following Armenia's independence, in 1996 we restarted our first detector—the Nor-Amberd Neutron Monitor 18NM64 (2000 m above sea level). A similar detector was commissioned and started to take data at the Aragats research station (3200 m above sea level) in 2000. The muon scintillation multi-directional monitor system started operation at the Nor-Amberd research station in 2002. A similar muon detector is arranged around the Mexico City neutron monitor, 6NM64 [16]. A Solar Neutron Telescope (SNT) is in operation at the Aragats station since 1997, as part of the worldwide network coordinated by the Solar-Terrestrial laboratory of the Nagoya University [17]. In addition to the primary goal of detecting the direct neutron flux from the Sun, the SNT also has the possibility to detect muon fluxes and roughly measure the direction of the incident muons. Another monitoring system is based on the scintillation detectors of the Extensive Air Shower

(EAS) surface arrays, MAKET-ANI and GAMMA, located on Mt. Aragats at 3200 m above sea level.

A flexible 32-bit microcontroller-based Data Acquisition (DAQ) electronics is designed to support the combined neutron–muon detector system and utilize the correlated information from cosmic ray secondary fluxes, including environmental parameters (temperature, pressure and magnetic field). Microcontroller-based DAQ systems and high precision time synchronization of the remote installations via Global Positioning System (GPS) receivers are crucial ingredients of the new muon facilities on Mt. Aragats in Armenia.

2. The Aragats Space Environment Center (ASEC)

The ASEC, [5] consists of two high-altitude stations on Mt. Aragats in Armenia. Geographic coordinates: 40°30'N, 44°10'E. Cutoff rigidity: ~7.6 GV, altitude 3200 m and 2000 m. At these stations, several monitors continuously measure the intensity of the secondary cosmic ray fluxes and send data to the Internet in real time. The specifications of the ASEC monitors are shown in Table 1. The two 18NM-64 NM [14], in operation at Nor-Amberd (2000 m elevation), and at Aragats, (3200 m elevation) research stations are called the Nor-Amberd Neutron Monitor (NANM), and the Aragats Neutron Monitor (ArNM), respec-

tively. The monitors are equipped with interface cards, providing time integration of counts from 1 s up to 1 min.

The SNT, is in operation at 3200 m above sea level at the Aragats research station. The main detecting volume consists of four 1-m² surface, 60-cm-thick scintillation blocks overviewed by photomultipliers type FEU-49 with 12-cm-large photocathode. The detecting volume is formed from standard 50 × 50 × 5 cm³ slabs, stacked vertically on the horizontal slab of 100 × 100 × 5 cm³ (total 164 slabs). Four, same-type scintillator slabs of 5-cm thick and 1-m² surface are located 1 m above the detecting volume (Fig. 1), with the goal to veto the near vertical charged flux. Total count rate of the veto detectors is also registered and reflects variations in the low-energy charged component. Incoming neutrons in nuclear reactions produce protons inside the thick scintillator target.

The probability to produce neutrons in 5 cm of scintillator is vanishingly small. The energy deposited due to ionization by protons is measured by photomultipliers over the scintillators. The signal amplitude of the photomultiplier output signals is discriminated according to four threshold values of 40, 80, 120 and 160 mV, corresponding to the threshold energies of 130, 240, 420 and 700 MeV, respectively. An independent registration channel (so called, 0-threshold channel) overviews the same scintillator slab and registers the charged and neutral components of secondary cosmic rays without veto and threshold options.

Table 1
Characteristics of the ASEC monitors

| Detector | Altitude, (m) | Surface area of scintillators (m ²) | Threshold(s) (MeV) | In operation since | Mean count rate (min ⁻¹) |
|-------------------|---------------|---|-------------------------|--------------------|--------------------------------------|
| NANM (18NM64) | 2000 | 18 | 100 | 1996 | 2.5×10^4 |
| ArNM (18NM64) | 3200 | 18 | 100 | 2000 | 6.2×10^4 |
| SNT-four | 3200 | Four 60-cm thick | 130, 240, 420, 700 | 1998 | 4.2×10^{4a} |
| Thresholds + veto | | Four 5-cm thick | 10 | | 1.2×10^5 |
| NAMMM | 2000 | 5 and 5 ^c | 10 and 350 ^c | 2002 | 2.5×10^{4b} |
| AMMM | 3200 | 48 | 5000 | 2002 | 1.2×10^{5b} |
| MAKET-ANI | 3200 | 6 × 16 groups | 10 | 1996 | 1.5×10^5 |

^aCount rate for the first threshold; near vertical charged particles are excluded.

^bTotal count rate of 48 muon detectors out of 100.

^cFirst value—surface and energy threshold for the upper detector, second value—bottom detector.

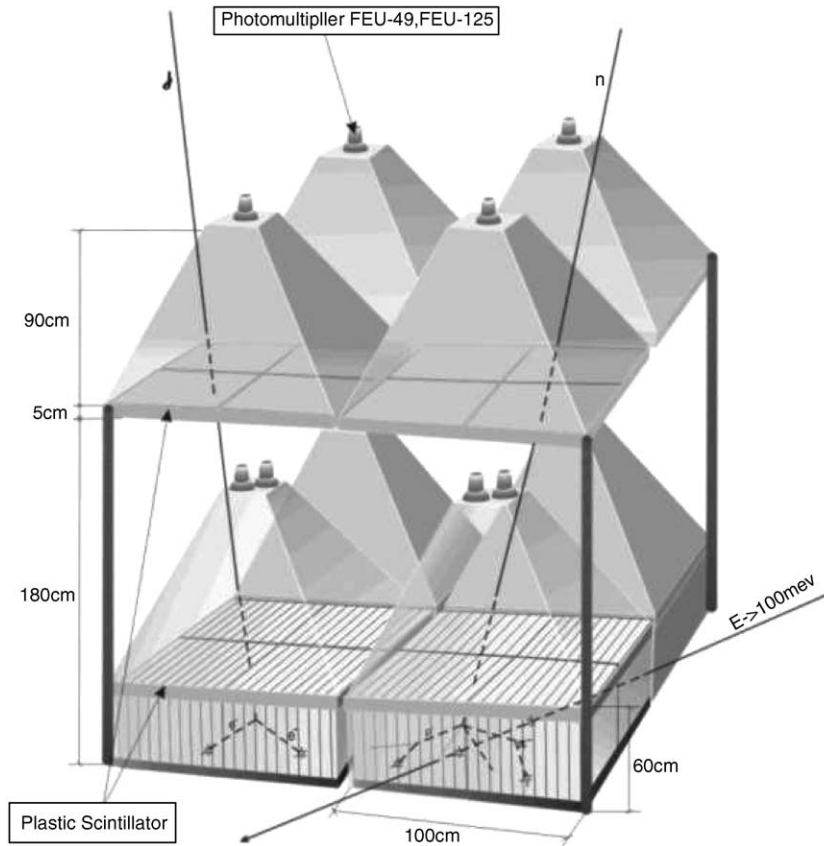


Fig. 1. Aragats Solar Neutron Telescope.

One of the advantages of the Aragats monitoring facilities includes registration of the muon flux under different angles of incidence. Simple coincidences techniques allow us to measure fluxes in 16 different combinations of triggered scintillation slabs, as it can be seen from Fig. 1. Four of these directions are vertical and also there are pairs of same angular acceptance. Therefore, nine independent directions of incidence can be outlined and used for the anisotropy measurements. Another advantage of the SNT is its connection to the MAKET-ANI surface detector [1,4]. As one can see from Fig. 1, all four 60 cm thick scintillators are overviewed with two photomultipliers. One group of detecting channels feed scalers via four discriminators; another group is equipped by logarithmic ADC and is triggered by the primary particles with energy greater than 5×10^{14} eV.

The Nor-Amberd Muon Multidirectional Monitor (NAMMM) [2,8], shown in Fig. 2 consists of two layers of plastic scintillators above and below one of the three sections of the NANM. The lead (Pb) filter of the NM absorbs electrons and low-energy muons. The threshold energy of the detected muons is estimated to be 350 MeV. The NAMMM consists of six up and six down scintillators, each having the area of 0.81 m^2 . The distance between layers is $\sim 1 \text{ m}$, and the mean angular accuracy is $\sim 25^\circ$. The DAQ system of the NAMMM can register all coincidences of detector signals from the upper and lower layers, thus, enabling measurements of the arrival of the muons from different directions. The signals ranging from 0.5 to 5 V, from each of the 12 photomultipliers, are passed to the programmable threshold discriminators. The discriminator output signals are

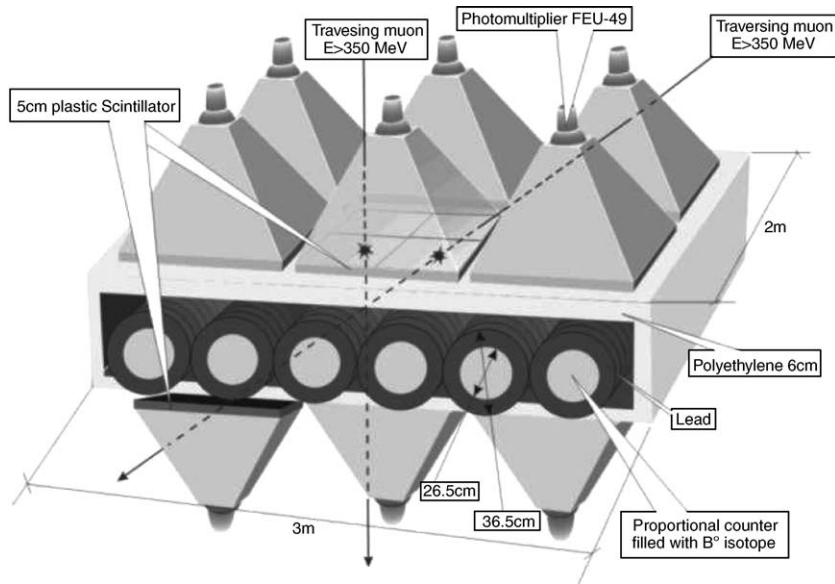


Fig. 2. Nor-Amberd Multidirectional Muon Monitor.

fed in parallel to the 12-channel OR gate triggering device and to a buffer.

Two 6-bit length words are stored in the buffer, reflecting the trigger status from the 12 registering channels: the first word is for the upper set and the second word is for the lower set. The ones correspond to “fired” channels and zeros to channels that were not fired during a program selectable duration gate in the range 100–1000 ns. The NAMMM triggered condition is defined by detecting at least one signal in the 12 data channels. The trigger rate of the entire detector system does not exceed 1.5 kHz. Taking into account that the gate width of the OR circuit is less than 1 μ s and the data arrival rate does not exceed 1.5 kHz, we can conclude, that the rate of random coincidences (uncorrelated signals in the upper and lower layers due to more than one near-horizontal muon traversing each layer) is insignificant. The 1- μ s-max output signal from the OR gate interrupts the microcontroller and triggers the data transfer from the buffer to the microcontroller RAM for on-chip data analysis. The duration of the entire data readout and signal processing procedure is less than 10 μ s. Therefore, detector dead time is negligible.

There are 43 different possibilities of so-called “basic states” of detector triggers. Thirty-six of them carry information about the direction of the incident muon. For example, trigger word configuration “001000” for the upper layer and “001000” for the lower layer corresponds to the muon traversal through third upper and third lower scintillators (zenith angle between 0° and 45°), as demonstrated in Fig. 2. Upper and lower layer trigger word configuration of “001000” and “100000”, respectively, corresponds to the traversal through the third upper and the first lower scintillator (zenith angle between 45° and 65°). The other seven possibilities, for example, more than one trigger in upper and lower layers such as “111100” and 110000”, respectively, or one in the upper layer and many in the lower layer, can be analyzed in terms of the various physical processes, such as the EAS hitting the detector setup, or particle generation in the lead (Pb) layer of the neutron detector system, neutron bursts (Stenkin, 2001), etc.

Events corresponding to each of the 43 basic states, described above, are independently summed over a 10-s data collection period. Then the string of the 10-s averaged 43 numbers is passed to the

analysis software and another cycle of 10-s summation is started. The sequence of the 10-s summation data is gathered for 5 min for a total of 30 number strings. The total amount of data from the 5-min integration time (30 sequences of 43 number strings, or 1290 numbers) is too large for storing on the chip. Therefore, we calculate 12×12 correlation matrices, to monitor how the correlations of count rates of the 12 detector channels are changing. The correlation matrix will provide a test for the random enhancements of the total detector count rate to spurious signals in one or more detector channels. The enhancement of the count rate in the detector due to changing geophysical conditions should be accompanied by the coherent enhancements of correlations between all (or vast majority) of the detecting channels. After completing the 5-min cycle, the computed means, standard deviations, and the correlation matrix are transferred to the on-line computer.

All electronics are of original design, according to modern very compact and high reliable technologies, oriented for easy maintenance and production. To minimize data transmission rate, the raw data is partially processed in microcontroller before sending it to the main computer. A 32-bit microcontroller is chosen as the basic element. Taking into account the slow data rates, and to minimize the cost, a serial data transmission is used instead of much more expensive parallel data transmission standards like CAMAC, VME, etc.

To guarantee the DAQ continuity, the electronics system is modernized gradually. A newly designed readout is based on the concept of full software control of the detector parameters and maximum utilization of all detector data. Each photomultiplier has its own local programmable high voltage (HV) power supply and buffer preamplifier to condition the pulses in preparation for sending them via long coaxial cables without degrading the dynamic range and signal-to-noise ratio. Counting modules are located in the counter room. They have buffer preamplifiers and programmable threshold comparators (discriminators) at the inputs. The threshold of the counter module input comparators can be programmed by

voltage and polarity in the range from -0.5 to 0.5 V. Besides the comparators, the buffer preamplifier output signals can be transferred to other data processing devices such as ADCs, etc., to be installed later. All electronics modules are based on using modern 8 and 32-bit microcontrollers, for the detector control system (HV programming and measurement) and for the main DAQ, respectively. Currently the Atmel 8-bit and Fujitsu FR 32-bit controllers are used.

The microcontroller-based electronics units (HV power supply and counting modules) have optional environmental sensors. The HV power supply has only temperature sensors, and the counting modules also have pressure and humidity sensors.

The main pressure sensor of the whole system is placed in a special pressure-tight box with possibility of periodic calibration using a standards Hg barometer. It consists of Motorola MPXA6115 Integrated Silicon Pressure Sensor and ATMEL 8-bit microcontroller and has frequency modulated output for direct coupling with counter modules and serial asynchronous interface to connect to the PC.

In the assembly of the ANI Cosmic Ray experiment [7], two detectors measuring the EAS are operated on the Aragats research station. The main goal of the GAMMA [9] and MAKET-ANI [1,4] detectors are to investigate the energy spectra of cosmic rays to understand the origin and accelerator mechanisms. Both detectors use the same particle density detection techniques to determine the number of electrons in the shower and infer the energy and type of the primary particle. EAS detectors are triggered arrays, but each detector counts all incident particles and an independent read-out stores the changing fluxes of charged particles. The count rates of the charged components at altitude 3200 a.s.l. are ~ 420 counts/ m^2/s for >10 MeV electrons and ~ 50 counts/ m^2/s for >5 GeV muons. These high count-rates, combined with the large area of the electron and muon detectors on Mt. Aragats, are very attractive for establishing a monitoring facility to investigate the correlations between variations of electron and muon count rates with the enhancing flux of solar ions incident on the Earth's atmosphere.

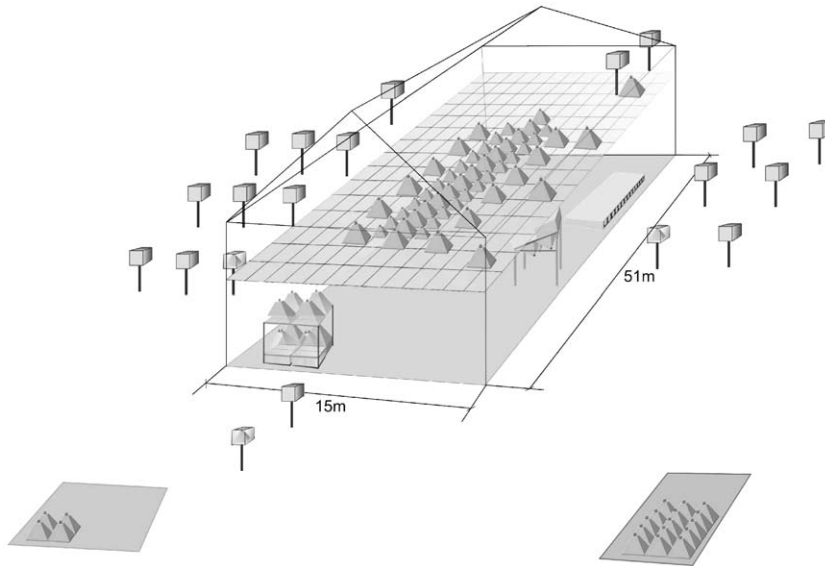


Fig. 3. MAKET-ANI Extensive Air Shower Detector.

The **MAKET-ANI** surface array, see Fig. 3, consists of 92 detectors formed from 5-cm-thick plastic scintillators, with area 1 m^2 each, to measure particle density of the registered EAS. Twenty-four of them have 0.09-m^2 area and 68 have 1-m^2 area. The central part consists of 73 scintillation detectors and is arranged in a rectangle of $85 \times 65\text{ m}^2$. In order to estimate the zenith and azimuthal angles, 19 detectors from the 92 are equipped with timing readout to measure the EAS front appearance with an accuracy of $\sim 5\text{ ns}$. The photomultipliers (PM-49) are placed in light-tight iron boxes. Logarithmic Analog to Digital Converters (ADC) and Constant Fraction Discriminators (CFD) are placed just above the photomultiplier. The dynamic range of the registered particle number is $\sim 5 \times 10^3$.

During multiyear measurements the detecting channels were continuously monitored. Data on background cosmic ray spectra was collected for each detector. The slope of the spectra was used for detector calibration. The slope of the background spectra is a very stable parameter which did not change even during very severe Forbush decreases, when the mean count rates can decrease as much as 20%. The changing fluxes of muons and electrons incident on the MAKET-ANI

detector are available from the MAKET-ANI data bank. All Forbush decreases and other geoeffective events are very well reproduced by these data with very good statistical provision; the 1-min count rate of the 1-m^2 plastic scintillator is $\sim 25\,000$.

One hundred and fifty plastic scintillators with area of 1 m^2 each are located in the underground hall of the ANI experiment, to measure the muon content of the EAS. The 6-m-thick concrete blocks plus the 7-m soil, filter the electrons and the low-energy muons. Thus, only muons with energies $> 5\text{ GeV}$ reach the detectors.

The Aragats Multidirectional Muon Monitor (**AMMM**) consists of 15 m^2 scintillation detectors, located on top of the ANI concrete calorimeter and 72 m^2 array (72 most reliable 1-m^2 detectors from 150) and the same type of detectors as 24m below, as shown in Fig. 4. Here, we can also see the modulation effects of the solar activity on the isotropic and uniform GCR filling interplanetary space. Protons hitting the shock from the back are reflecting those forming the “depletion” region behind the shock. Protons hitting the approaching shock front, *visa-versa*, can enhance flux of particles in the definite directions. Both effects can form “precursors” of upcoming geomagnetic

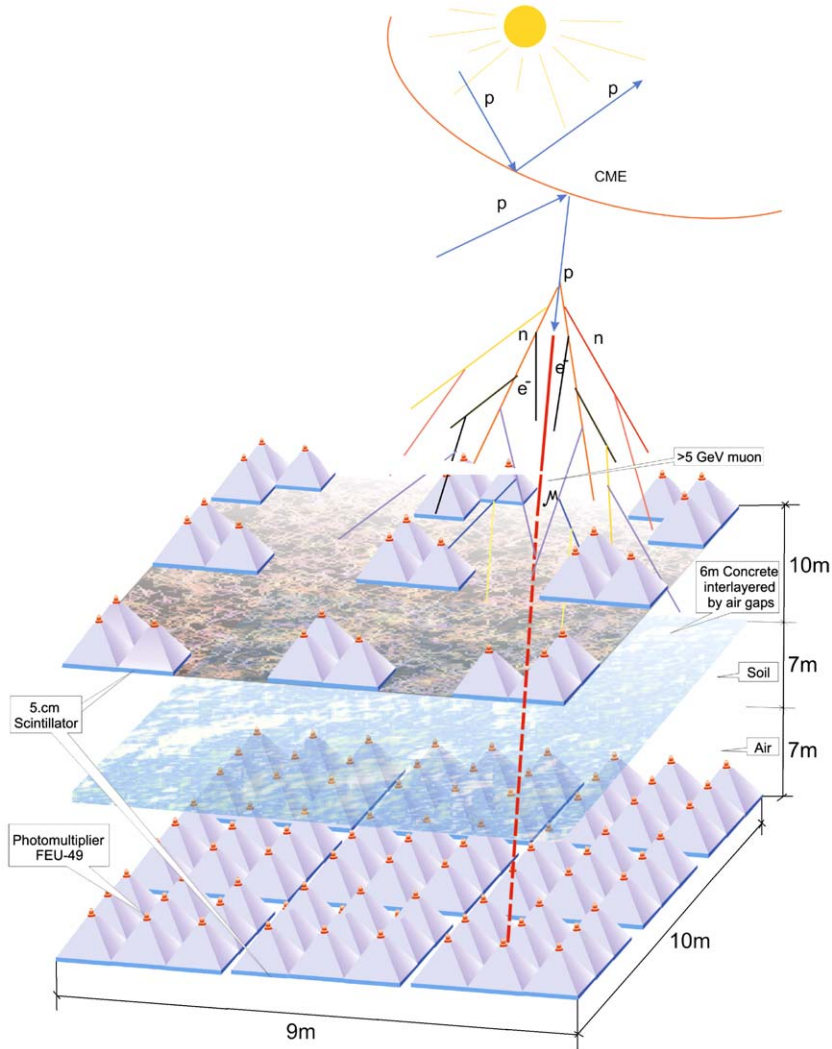


Fig. 4. Aragats Multidirectional Muon Monitor.

storm and can be detected by the ground-based monitors far before start of the storm [13]. From the same figure we can see the production of the secondary particles in interactions of the primary proton with earth's atmosphere. If energy of primary proton is enough, numerous secondary particles are born and, some of them can reach the mountain altitudes and be registered by the ASEC monitors.

Using the coincidence technique, we can monitor changing count rates from numerous space directions. Detectors on the top are grouped in

three, while those in the underground hall are grouped in eight to provide significant amount of coincidences. The geometry of the detector arrangement will allow us to detect particles arriving from the range of directions from vertical to 60° declination, with the accuracy of $\sim 10^\circ$, with very good statistics.

By measuring the intensity deficit of the GCR, it will be possible to determine the loss cone direction and perform "screening" of the approaching magnetized plasma cloud. The worldwide network of muon monitors, covering as many

incident directions as possible, could be used for the early forecasting of the upcoming severe geomagnetic storm [15]. The lower layer of the AMMM constitutes a very sensitive high-energy muon monitor, robust to local atmospheric conditions because of the rather high-energy threshold. The total count rate of the monitor is approximately $\sim 200\,000/\text{min}$. Thus, the sensitivity of this monitor reaches record value of $\sim 0.2\%$ for 1 min count rates, three times better than the Aragats NM.

Simultaneous detection of variations in low-energy charged particles, neutron, and high-energy muon fluxes by the ASEC monitors will provide new possibilities for investigating the transient solar events and will allow us to classify Geoeffective events according to their physical nature and magnitude.

3. Correlation analysis of ASEC monitors recordings

The biggest Forbush decrease from 29 October 2003 was detected by all ASEC monitors.

From Figs. 5–14, we can see that on 29 October 2003 the neutron flux is attenuated by 20%, low-energy charged particle flux by 15% and high-energy muons by 7–8%. The relative values of flux attenuation in different components of the secondary cosmic ray flux can be used as a characteristic of the Fd magnitude. For the investigation of parameters of secondary fluxes, which are the most sensitive to the geoeffectiveness of the event, we select four distinct test cases: one corresponding to the silent phase of the geomagnetic disturbance, and others corresponding to the

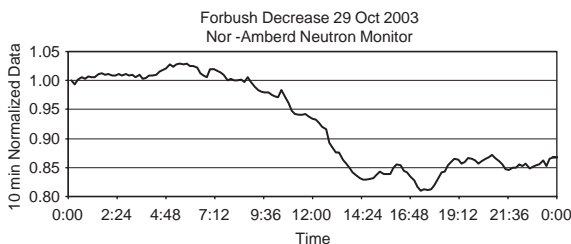


Fig. 5. Forbush decrease; neutrons, 3200 m.a.s.l.

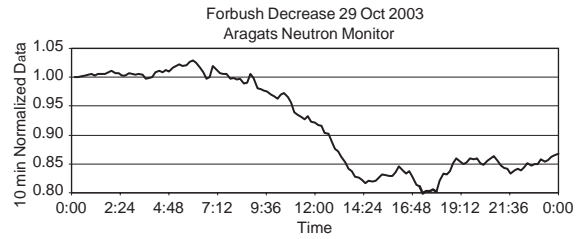


Fig. 6. Forbush decrease; neutrons, 2000 m.a.s.l.

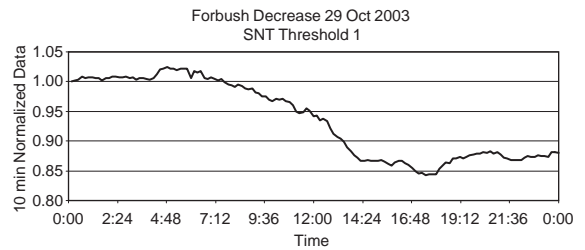


Fig. 7. First threshold of SNT.

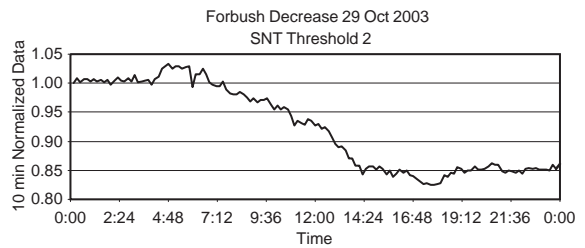


Fig. 8. Second threshold of SNT.

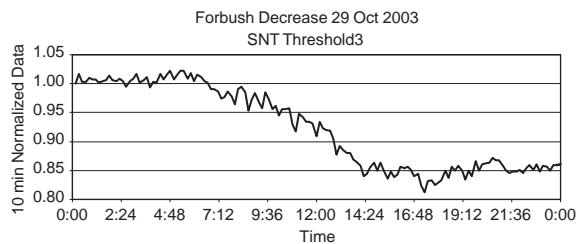


Fig. 9. Third threshold of SNT.

Fd of different magnitudes—from modest, to strongest. The selected cases are: 25 January 2004, 20 November 2003, 27 July 2004 and 29 October 2003. Correlation matrices of these events are presented in Tables 2–5.

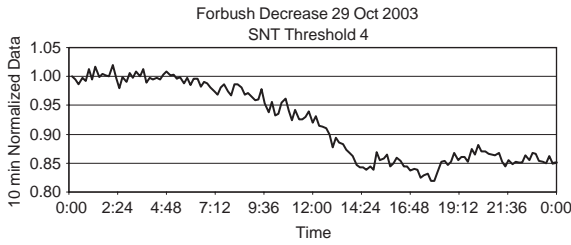


Fig. 10. Forth threshold of SNT.

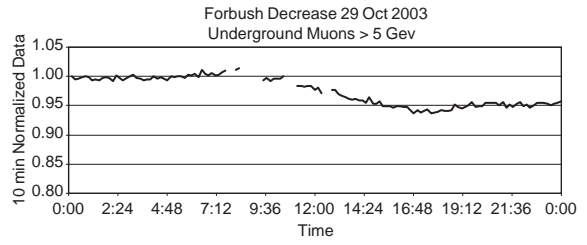


Fig. 14. Fd in 5 GeV muons; 5-cm-thick scintillator.

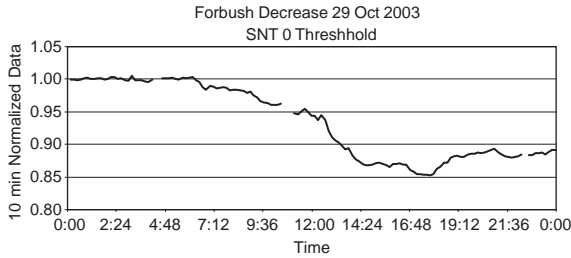


Fig. 11. Fd in low-energy charged particles; 60-cm-thick scintillator.

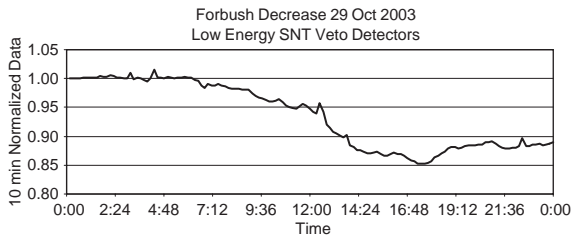


Fig. 12. Fd in low-energy charged particles; 5-cm-thick scintillator, VETO detector.

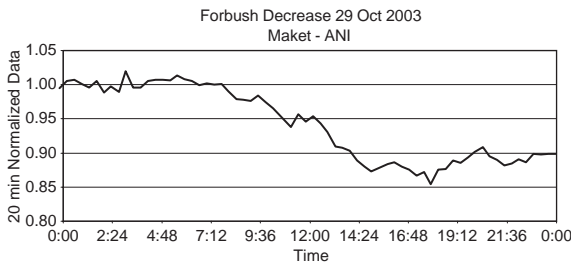


Fig. 13. Fd in low-energy charged particles; 5-cm-thick scintillators, MAKET ANI detector.

Correlations between different particle fluxes calculated for 25 January 2003, when no geomagnetic activity was detected are presented in Table 2. As it is expected, there are no correlations between different monitor recordings. Only SNT of different thresholds display correlation with each other, because if the particle has enough energy to trigger threshold 4, it triggers all lower thresholds as well, and all thresholds react on the one and the same particle.

For 29 October 2003 Fd, very strong correlations between all monitors are seen (Table 5), which indicates that the magnetic field of the CME has influence on the particles of all energies (up to ~50 GeV—the median value of the primary proton energy generating 5 GeV muons), so that all monitor count rates are decreasing similarly.

For smaller events of 27 July 2004 and 20 November 2003 (Tables 3 and 4) it is seen that the correlations between monitor count rates are large for the low-energy particles and they are decreasing with energy. Correlation with four energy thresholds of SNT is gradually decreasing from 0.75 down to 0.32.

Now we will try to illustrate how the calculated correlation coefficients are related to the geoeffectiveness of the event. As a geoeffectiveness characteristic, we choose the Disturbance storm time (Dst), which is a geomagnetic index, indicating the world magnetic disturbance level. The index is constructed by averaging the horizontal component of the geomagnetic field from mid-latitude and equatorial magnetometers from all over the world.

In Table 6 we present the correlation coefficients of the above-mentioned four events with corresponding detected minimal values of the Dst.

Table 2

Correlations between different ASEC monitor recordings for 25 January 2003 (the case of absence of any geomagnetic activity)

| | ArNM | NANM | SNT thr0 | SNT thr1 | SNT thr2 | SNT thr 3 | SNT thr4 | Muons>5 Gev |
|-------------|------|-------|----------|----------|----------|-----------|----------|-------------|
| ArNM | 1 | | | | | | | |
| NANM | 0.01 | 1 | | | | | | |
| SNT thr0 | 0.02 | -0.01 | 1 | | | | | |
| SNT thr1 | 0.05 | 0.03 | 0.06 | 1 | | | | |
| SNT thr2 | 0.04 | -0.04 | -0.05 | 0.43 | 1 | | | |
| SNT thr3 | 0.03 | 0.03 | -0.01 | 0.31 | 0.42 | 1 | | |
| SNT thr4 | 0.03 | 0.02 | 0.01 | 0.22 | 0.24 | 0.21 | 1 | |
| Muons>5 Gev | 0.03 | 0.02 | 0.12 | 0.08 | -0.04 | 0.00 | 0.01 | 1 |

Table 3

Correlations between different ASEC monitor recordings for the Forbush decrease of 20 November 20 2003 event (from 10:00 to 12:00 UT)

| | ArNM | NANM | SNT thr0 | SNT thr1 | SNT thr2 | SNT thr 3 | SNT thr4 | Muons>5 Gev |
|-------------|------|------|----------|----------|----------|-----------|----------|-------------|
| ArNM | 1 | | | | | | | |
| NANM | 0.72 | 1 | | | | | | |
| SNT thr0 | 0.75 | 0.76 | 1 | | | | | |
| SNT thr1 | 0.69 | 0.72 | 0.88 | 1 | | | | |
| SNT thr2 | 0.62 | 0.63 | 0.75 | 0.81 | 1 | | | |
| SNT thr3 | 0.41 | 0.47 | 0.52 | 0.56 | 0.68 | 1 | | |
| SNT thr4 | 0.32 | 0.37 | 0.36 | 0.40 | 0.48 | 0.68 | 1 | |
| Muons>5 Gev | 0.38 | 0.43 | 0.48 | 0.45 | 0.42 | 0.28 | 0.12 | 1 |

Table 4

Correlations between different ASEC monitor recordings for the Forbush decrease of 27 July 2004 event (from 0:00 to 24:00 UT)

| | ArNM | NANM | SNT thr0 | SNT thr1 | SNT thr2 | SNT thr 3 | SNT thr4 | Muons>5 Gev |
|-------------|------|------|----------|----------|----------|-----------|----------|-------------|
| ArNM | 1 | | | | | | | |
| NANM | 0.93 | 1 | | | | | | |
| SNT thr0 | 0.92 | 0.89 | 1 | | | | | |
| SNT thr1 | 0.89 | 0.86 | 0.94 | 1 | | | | |
| SNT thr2 | 0.75 | 0.72 | 0.83 | 0.90 | 1 | | | |
| SNT thr3 | 0.62 | 0.59 | 0.66 | 0.71 | 0.79 | 1 | | |
| SNT thr4 | 0.45 | 0.43 | 0.47 | 0.50 | 0.56 | 0.70 | 1 | |
| Muons>5 Gev | 0.85 | 0.84 | 0.83 | 0.81 | 0.66 | 0.52 | 0.37 | 1 |

From Fig. 15 it is apparent that a strong association exists between selected correlation coefficients and corresponding values of Dstmin.

Thus, the correlation matrixes contain valuable information on the geoeffectiveness of the event: the higher correlation coefficient between ArNM

and AMMM, and/or between ArNM and SNT, the stronger is the geomagnetic disturbance.

We performed also correlation analysis of the 20 November 2003 huge geomagnetic storm.

In Fig. 16 we see large enhancement of the Neutron Monitor count rates accompanied by

Table 5

Correlations between different ASEC monitor recordings for the Forbush decrease of 29 October 2003 event (from 6:00 to 14:40 UT)

| | ArNM | NANM | SNT Thr 0 | SNT Thr 1 | SNT Thr 2 | SNT Thr 3 | SNT Thr 4 | Muons > 5 Gev |
|---------------|------|------|-----------|-----------|-----------|-----------|-----------|---------------|
| ArNM | 1 | | | | | | | |
| NANM | 1.00 | 1 | | | | | | |
| SNT Thr 0 | 0.99 | 0.99 | 1 | | | | | |
| SNT Thr 1 | 0.99 | 0.99 | 1.00 | 1 | | | | |
| SNT Thr 2 | 0.99 | 0.99 | 0.99 | 1.00 | 1 | | | |
| SNT Thr 3 | 0.98 | 0.98 | 0.99 | 0.99 | 0.99 | 1 | | |
| SNT Thr 4 | 0.98 | 0.98 | 0.99 | 0.99 | 0.99 | 0.99 | 1 | |
| Muons > 5 Gev | 0.97 | 0.97 | 0.97 | 0.97 | 0.97 | 0.96 | 0.95 | 1 |

Table 6

Correlation coefficients and minimal values of Dst for different event

| Event | Correlation coefficient between ArNM and AMMM | Correlation coefficient between ArNM and SNT_0 | Dstmin (nT) |
|------------------|---|--|-------------|
| 25 January 2004 | 0.03 | 0.02 | -20 |
| 20 November 2003 | 0.38 | 0.75 | -84 |
| 27 July 2004 | 0.85 | 0.92 | -236 |
| 29 October 2003 | 0.97 | 0.99 | -360 |

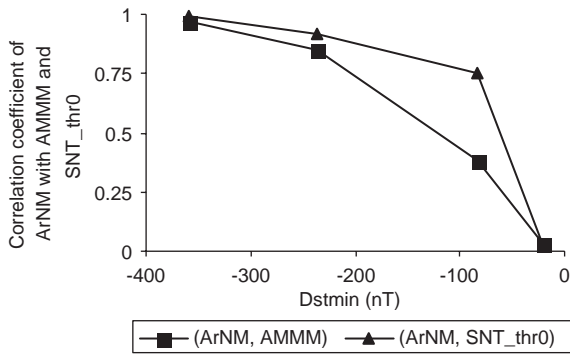


Fig. 15. Correlation coefficients between neutrons and high-energy muons (ArNM, AMMM) and between neutrons and low-energy charged particles (ArNM, SNT_0threshold) versus minimal value of Dst.

much smaller enhancement of the low-energy charged component and, stable count rate of the high-energy muons.

To characterize the magnitude of the geoeffectiveness of the event, we again use the Dst index. During this storm the Dst index decreased by as much as a record value of -472 nT. Interaction of the arriving shock with the geomagnetic field led to the significant reduction of geomagnetic cutoff at the Mt. Aragats latitude. The correlation matrix for this event is presented in Table 7.

One can see that for the geomagnetic storm of 20 November 2003 the correlation between ArNM and NANM is strong (~ 0.9), because these two instruments of the same type are registering neutron flux, originated by low-energy primaries. The different location levels cause the differences in these monitors' recordings. Some secondary neutrons from low-energy primaries, which are registered by ArNM, are missed in NANM, because they do not reach the NANM level (2000 m a.s.l.). There is also a strong correlation between the neutron flux and the charged component flux (mostly electrons and low-energy muons). High-energy muons did not correlate with neutrons. To reproduce this correlation pattern, we perform simulations of the time series of different secondary cosmic rays. We take into account as CR propagation through the Earth's atmosphere using CORSIKA code [10] and also detector response according to Ref. [6]. The median energies of primary protons, originating as minimum one neutron or low-energy charged particle in the secondary flux are ~ 10 – 20 GeV, while high-energy muons are originated by protons with median energy of ~ 50 GeV. This conclusion follows from Fig. 17, where three simulated distributions represent the normalized

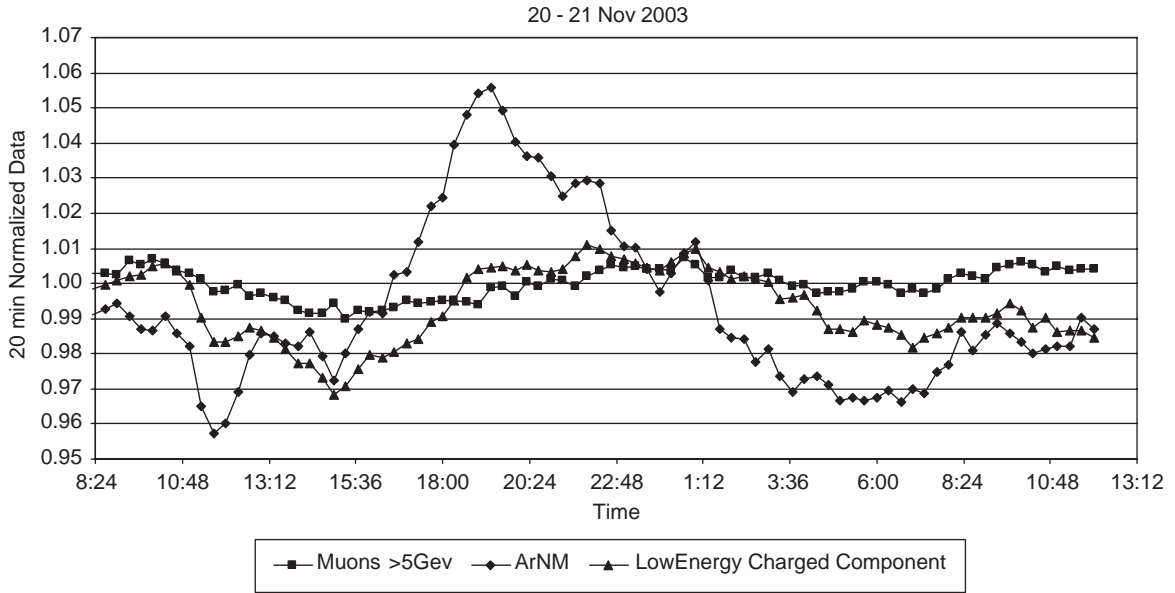


Fig. 16. Time profile of particles observed by ASEC monitors on 20 November 2003.

Table 7

Correlations between different ASEC monitors recordings for the geomagnetic storm of 20 November 2003 event (from 14:40 to 6:00 UT, 21 November)

| | ArNM | NANM | SNT thr0 | SNT thr1 | SNT thr2 | SNT thr 3 | SNT thr4 | Muons > 5 Gev |
|---------------|-------|-------|----------|----------|----------|-----------|----------|---------------|
| ArNM | 1 | | | | | | | |
| NANM | 0.89 | 1 | | | | | | |
| SNT thr0 | 0.47 | 0.44 | 1 | | | | | |
| SNT thr1 | 0.81 | 0.79 | 0.64 | 1 | | | | |
| SNT thr2 | 0.85 | 0.83 | 0.34 | 0.82 | 1 | | | |
| SNT thr3 | 0.67 | 0.65 | 0.44 | 0.70 | 0.76 | 1 | | |
| SNT thr4 | 0.38 | 0.35 | 0.34 | 0.43 | 0.43 | 0.67 | 1 | |
| Muons > 5 Gev | -0.01 | -0.04 | 0.44 | 0.14 | -0.04 | 0.13 | 0.13 | 1 |

energy spectra of primary protons originating at least one neutron, one electron or muon, and one muon of high energy at detection altitude of 3200 m. Therefore, the primary protons from the left tails of the mentioned distributions will enter the atmosphere and generate additional particles detected by NMs and lower channels of SNT. The distribution of the protons generating the high-energy muons is shifted to the right on the energy scale, and decrease of the geomagnetic cutoff cannot influence the count rate of high-energy muons.

4. Conclusion

We have demonstrated the sensitivity of correlation analysis to the different types of events, which cause strong geomagnetic disturbances. We conclude that the correlations between different ASEC monitor count rates could be used for the identification of geoeffectiveness of events according to their type and severity. The possibility of the early diagnosis of the expected hazard from geomagnetic and/or radiation storms, using the correlation information on the changing

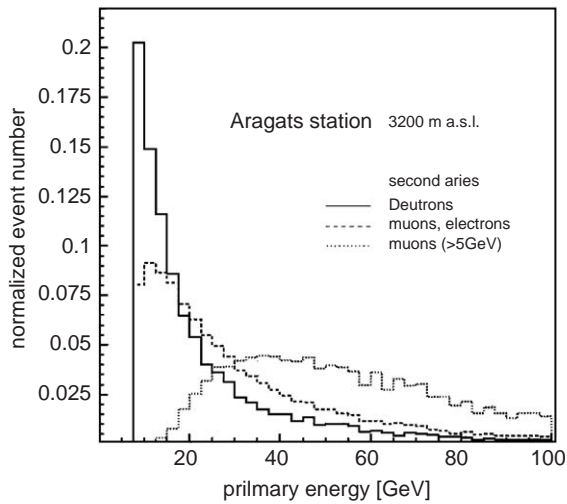


Fig. 17. The normalized event numbers of primary particles originating different secondary particle fluxes.

fluxes of the ASEC monitors, is under investigation now.

Acknowledgement

The data collected by the ASEC detectors are the property of the ASEC collaboration. The SNT detector is part of Solar Neutron Telescopes World-wide network, coordinated by Prof. Muraki's group from Solar–Terrestrial Laboratory of Nagoya University. The authors also thank CRD staff for fruitful collaboration. Work was supported by Armenian government grants, by grant ISTC A1058, and by grant INTAS IA-2000-01.

References

- [1] V.V. Avakian, E.B. Bazarov, et al., VANT, ser. Tech. Phys. Exp. 5 (31) (1986) 1.
- [2] A.S. Beglaryan, S.P. Bujukyan, et al., Scientific publication of YerPhi 1197(74) 1989.
- [3] A.V. Belov, J.W. Bieber, E.A. Eroshenko, et al., Adv. Space Res. 31 (4) (2003) 919.
- [4] A.A. Chilingarian, et al., Proceedings of the 24th International Cosmic Ray Conference, Salt Lake City, vol. 1, 1999, p. 240.
- [5] A. Chilingarian, K. Avakyan, et al., J. Phys. G 29 (2003) 939.
- [6] J.M. Clem, L.I. Dorman, Space Sci. Rev. 93 (2000) 335.
- [7] T.V. Danilova, et al., Nucl. Instr. and Meth. A 323 (1992) 104.
- [8] L.L. Dorman, Variations of the Galactic Cosmic Rays, Publishing house of the Moscow State University, Moscow, 1975.
- [9] A.P. Garyaka, R.M. Martirosov, et al., J. Phys. G 28 (2002) 2317.
- [10] D. Heck, et al., Forschungszentrum Karlsruhe, FZKA Report 6019, 1998
- [11] K. Kudela, M. Storini, M.Y. Hofer, A.V. Belov, Space Sci. Rev. 93/1–2 (2000) 153.
- [12] K. Kudela, R. Brenkus, J. Atmos. Solar Terr. Physics 66 (2004) 1121.
- [13] T. Kuwabara, K. Munakata, et al., Geophys. Res. Lett. 31 (2004) L19803.
- [14] H. Moraal, A. Belov, J.M. Clem, Space Sci. Rev. 93 (2000) 285.
- [15] K. Munakata, J.W. Bieber, S. Yasue, et al., J. Geophys. Res. 105 (2000) 27,457.
- [16] Y.V. Stenkin, J.F. Valdes-Galicia, et al., Astroparticle Phys. 16 (2001) 157.
- [17] H. Tsuchiya, Y. Matsubara, et al., Detection Efficiency of a new type of Solar Neutron Detector calibrated by an accelerator Neutron Beam, Nucl. Instr. and Meth. A 463 (2001) 183.